Clays and Clay Minerals, Vol. 68, No. 1:9–22, 2020

SURFACE CHEMISTY, MICROSTRUCTURE, AND RHEOLOGY OF THIXOTROPIC 1-D SEPIOLITE GELS

Pengfei Liu[1], Mingyong Du[1], Peta Clode[2], Hualong Li[1], Jishan Liu[1], and Yee-Kwong Leong[1]*

[1]Department of Chemical Engineering, The University of Western Australia, 35 Stirling Highway, Crawley, WA 6009, Australia
[2]Centre for Microscopy, Characterization and Analysis, The University of Western Australia, 35 Stirling Highway, Crawley, WA 6009, Australia

Abstract—The rheological properties of sepiolite gels in relation to solution chemistry, fiber charge, and microstructure are poorly understood. The purpose of this study was to bring more clarity to this topic by quantifying the effects of solution pH, ionic strength, and adsorbed tetrasodium pyrophosphate (TSPP) additive on rheological properties. The electrical charge on sepiolite fibers was investigated to explain the fiber interaction configuration observed in the microstructure. Fiber interaction forces and dynamics explained the ageing behavior of the gel. Sepiolite gels of only a few percent solids displayed long-time ageing behavior, which was manifested by an increasing yield stress with wait time and continued for weeks. The gel microstructure showed randomly orientated rigid fibers with cross configuration attraction. Each fiber experiences both attractive (van der Waals and heterogeneous charge) and repulsive (electric double layer) forces, and initially a net force. The repulsive force causes these fibers to orientate or move continually to achieve a state of force equilibrium and this process takes a long time. The Leong model describes this ageing behavior. For good fiber separation, high intensity probe sonication of the suspension was required. The yield stress increased with sonication time, solids loading, and temperature. The yield stress was absent at pH > 11 and increased to a maximum value at pH < 8. This maximum was insensitive to pH between 4 to 8, and ionic strength up to 1 M KCl. TSPP reduced this maximum and shifted the zero yield stress region to a lower pH, ~7. The zero yield stress state corresponded to a zeta potential with a minimum magnitude of 30 mV.

Keywords—1-D material · Ageing · Dispersion · Drilling fluids · Microstructure · Temperature

INTRODUCTION

The rheology of aqueous fiber suspensions where colloidal forces are important has been studied quite extensively (e.g. Solomon & Boger 1998; Djalili-Moghaddam & Toll 2005; Wolf et al. 2007; Bounoua et al. 2016). Most of these studies involved fibers with homogeneous surface properties in terms of the type of the surface charge. In contrast, clay minerals including fibrous sepiolite and palygorskite, displayed inhomogeneous charge properties with negative face and positive edge charges. For Na-montmorillonite and hectorite, this heterogeneous charge was a factor responsible for the long-time ageing behavior (Du et al. 2018; Leong et al. 2018). Their artefact-free cellular or sponge-like microstructures responsible for this behavior were captured by cryo-SEM. Rod-like sepiolite and palygorskite suspensions also displayed thixotropic behavior at very low solids loadings (Neaman & Singer 2000; Tunc et al. 2011).

Neaman & Singer (2000) used the rheogram hysteresis loop area to study the thixotropic property of palygorskite suspensions. This area quantifying the thixotropic property was related to ageing time, pH, and ionic strength. This method is not suitable for a long ageing-time study because of the logistics and handling issues of suspensions aged for long periods. Keeping the suspension in the concentric cylinder of the rheometer for days or weeks is problematic and drying of the sample cannot be avoided. If the sample is kept externally in an airtight container, the transfer of the aged gel to a measuring cup will lead to significant and uncontrollable structural damage. Neaman & Singer (2000) also presented SEM images showing the microstructure of dried suspension samples at various pH values. They do not represent the true microstructure in the suspension. To capture the artefact-free microstructure, the gel sample must be treated at very high pressure and subjected to rapid freezing (Du et al. 2018; Leong et al. 2018).

Most studies of clay-gel thixotropy have focused on short-time ageing behavior involving minutes or hours (Joshi et al. 2008; Tunc et al. 2011; Shu et al. 2015). Most conventional viscometric characterization methods, such as the dynamic storage modulus and the flow loop, are unsuitable for long-time ageing characterization. The vane technique can, however, measure directly the yield stress of a sample kept in any container (de Kretser & Boger 2001; Chang & Leong 2014). Two recent studies highlighted the long duration (days) of the particulate processes in resting clay gels (Du et al. 2018; Leong et al. 2018). Artefact-free microstructures of Na-montmorillonite and hectorite clay gels associated with this long-time ageing behavior revealed interesting features such as cellular or sponge-like microstructure, platelet size, and interaction configuration. Platelet interaction configurations and the nature of surface forces responsible for this microstructure were uncovered based on knowledge of the charge properties and morphology of the clay platelet and the microstructure information. Clay morphology, such as platelet or nano-disk, affected the microstructure formed (Du et al. 2018; Leong et al. 2018). This study on fibrous or 1-D sepiolite with heterogeneous charge property should produce information leading to a more complete understanding of the effect of clay morphology and charge properties on the long-time ageing process and the microstructure formed.

The open cellular microstructure of thixotropic clay gels showed that platelets are participating in both attractive and

* E-mail address of corresponding author: yeekwong.leong@uwa.edu.au
DOI: 10.1007/s42860-019-00050-z

repulsive interactions (Du et al. 2018, 2019; Leong et al. 2018). The platelets of Na-montmorillonite and natural hectorite were only a few nanometers thick and several hundreds of nanometers long or wide, and highly flexible. The platelet–platelet bond is formed by heterogeneous charge and van der Waals attraction in the overlapping edge-face and edge-edge configurations. The separation distance between the interacting faces at the bond should be much less than 1 nm, so the van der Waal force contribution to the bond strength should be significant. The network junctions of the 3-D microstructure are formed by attractive interactions in the overlapping edge-face configuration. The repulsive interaction between the faces of interacting platelets opens up the structure. However, with the nano-discotic synthetic hectorite gel, Du et al. (2018) showed irrefutable evidence of microstructure being formed by sheets instead of primary nano-disks (25 nm in diameter and 1 nm thick) particles. These disks interact attractively in an overlapping edge-edge configuration to form the 100–200 nm sheet. This microstructure contradicts the prevailing model that the 3-D microstructure is formed by primary disk particles interacting in the edge-face or card-house configuration (Dijkstra et al. 1997; Odriozola et al. 2004; Joshi et al. 2008; Ruzicka et al. 2011; Suman & Joshi 2018). The global free energy of this card-house microstructure formed by primary disks is not at a minimum. The disk-disk repulsive interaction must be strong due to their close proximity in this microstructure. The 3-D microstructure formed by 100–300 nm sheets is thus energetically more favorable as their face-face separation distance is much further apart. This result also highlights the inadequacy of disk pair interaction modeling in predicting the 3-D microstructure (Dijkstra et al. 1997; Odriozola et al. 2004). Multibody interaction modeling may be necessary to capture the essential, missing physics. Such modeling involving long-range van der Waals and electrostatic forces should pose a very interesting challenge to theoretical physicists. Definitive information on the platelet interaction configuration and microstructure may help with the simplification of the problem. With sepiolite, the information on fiber interaction configuration is currently not available and this can be acquired from the artefact-free microstructure collected in this study.

Sepiolite has many commercial applications. It is used in drilling muds, paper coating, adhesives, ceramics, refractories, rubbers, pharmaceuticals, animal nutrition, catalyst, adsorbents, and cosmetics (Alvarez et al. 1984; Galan 1996; Murray 2000). One of the largest uses is as viscosity builders in drilling muds. An essential function is that sepiolite additive should form a strong gel structure at rest, so as to hold the cuttings and weighing materials in suspension should the mud circulation cease (Sehly et al. 2015). The thixotropic behavior of an increasing viscosity and yield stress with rest time ensures that the cuttings and weighing materials remained suspended. Its shear-thinning or pseudo-plastic property is also beneficial in terms of suspension stability and spread ability. The sharp viscosity decrease with shear facilitates manual as well as mechanical spreading and leveling. The major advantages of sepiolite-based drilling muds over bentonite-based drilling muds are their insensitivity to electrolytes and high temperature (Murray 2000). Sepiolite is the only clay mineral that is stable at high temperatures and for this reason it is also used in drilling muds for geothermal wells. Moreover, sepiolite does not require osmotic swelling for gelling and so it can be prepared in organic solvents without concern for the exchangeable cation or electrolyte chemistry. This unique property gives sepiolite a greater versatility in drilling-mud formulation (Alverez et al. 1984; Galan 1996). Tools to control easily the rheology of drilling muds are essential in order to meet the requirements of the drilling environment. Adsorbed additives, pH, and ionic strength are such tools (Leong et al. 1993a, 1995; Johnson et al. 2000; Borgnino 2013). These are surface chemistry tools and they govern the nature and strength of the surface forces operating in a colloidal suspension which, in turn, determine its rheological behavior (Larson 1999). A range of surface forces can be exploited and these are van der Waals, electric double layer (EDL), steric, bridging, patch charge, hydrophobic, hydrogen bond, and depletion (Guven 1992a; Leong et al. 1993a; Leong & Ong 2015). Anionic adsorbed additives such as tetrasodium pyrophosphate (TSPP) can also be used to establish the presence of positive charge sites on net negatively charged clay minerals. The purpose of this study was to gain a better understanding of the effects of TSPP, pH, and ionic strength on rheological behavior of sepiolite by examining these properties in more detail.

MATERIALS AND METHODS

Materials and Preparation of Sepiolite Suspension

The sepiolite, a hydrated Mg phyllosilicate, used in this study was Pangel S9 provided by TOLSA Group (Madrid, Spain). It came from the Vallecas-Vicalvaro clay deposits in Spain and has a purity of >95% (Castro-Smirnov et al. 2017).

It was dried in an oven at l05°C for 24 h to remove adsorbed moisture before being used for suspension preparation. The sepiolite suspensions were prepared by first mixing accurately known amounts of Pangel S9 and deionized water in a 75 mL screw-top translucent plastic container and then sonicating the mixture with a high intensity probe. A previous study showed that high shear is necessary for fully dispersing sepiolite in water (Simonton et al. 1988). Therefore, a Branson sonifier (400 W, 20 kHz) with a one-inch probe was used to produce a homogeneous suspension. The sonifier manufactured by Branson Ultrasonics (Danbury, Connecticut, USA) was operated at an amplitude of 70%. The suspension was treated for 1 min and then rested for 2 min to allow the suspension to cool down. The process was repeated until the sepiolite particles were fully dispersed. The (4 wt.%) sepiolite suspension displayed a natural pH of 8.5 and electric conductivity of ~0.1 mS/cm.

Tetrasodium pyrophosphate (TSPP, $Na_4P_2O_7{\cdot}10H_2O$) of ACS reagent grade (≥99%) was purchased from Sigma-Aldrich (Castle Hill, NSW, Australia). The concentration of TSPP was reported on a dry weight basis (dwb.% - g additive/100 g sepiolite). Analytical grade (AR) KCl, HNO_3, and NaOH reagents were used.

https://doi.org/10.1007/s42860-019-00050-z Published online by Cambridge University Press

Characterization of Surface, Flow, and Ageing Properties

The zeta potential of the clay suspensions was characterized using a ZetaProbe (Colloidal Dynamics Inc., Ponte Vedra Beach, Florida, USA). To obtain the relationship between zeta potential and pH, a dilute sepiolite suspension (0.3 wt.%) prepared at pH~12 was potentiometrically titrated. The direction of the pH change was from high to low using 0.57 M HNO_3 as the titrant.

The pH and conductivity of suspensions were measured using an Orion 4-Star pH-conductivity meter manufactured by Thermo Fisher Scientific (Waltham, Massachusetts, USA).

The yield stress of the suspensions was measured using the vane technique (Nguyen & Boger 1985). Two vane viscometers, Brookfield RVDV-II + PRO and LVDV-II + PRO (AMETEK Brookfield, Middleboro, Massachusetts, USA), with different spring constants, were used. The RVDV viscometer is suitable for yield stress >100 Pa and the LVDV instrument provides accurate measurements for yield stress in the 1–100 Pa range. The pH of the suspensions was changed in a stepwise manner by adding 1 M NaOH or 1 M HNO_3 in a dropwise manner.

The flow behavior of the suspension was characterized with a MCR72 rheometer (Anton Paar GmbH, Graz, Austria). A cone-and-plate geometry (diameter = 50 mm, cone angle = 1°) was used. The direction of shear rate application was from high to low, 1000 s^{-1} to 10 s^{-1}. A 30 s pre-shear time at 1000 s^{-1} was applied prior to each characterization.

In the ageing study, the freshly prepared suspensions were left at rest for a few days. This step allows surface transport processes such as hydration, charging, and ion transport to reach a state of surface chemical equilibrium (SCE). This SCE state was determined from the relationship between the yield stress of vigorously stirred suspension and time since preparation. The SCE state was reached when the yield stress of the structural breakdown state attained a constant value (Du et al. 2018; Leong et al. 2018). Upon reaching this state, the ageing or structural recovery experiment was commenced immediately. During ageing no shearing or agitation was permitted. The yield stress was measured at different locations in the gel and at different ageing times. The first point in the ageing curve, representing the yield stress at zero ageing time, was measured immediately after the suspension was agitated vigorously. During ageing, each yield stress measurement was conducted in an area not disturbed by a previous measurement. A very small vane with a diameter of 0.6 cm and 1.2 cm long was used so that many measurements could be performed in undisturbed areas.

Scanning Electron Microscopy of Sepiolite Particles and Sepiolite Suspension

The morphology of the sepiolite particles was imaged using a Zeiss 1555 variable pressure field emission scanning electron microscope (Carl Zeiss Microscopy GmbH, Jena, Germany). The particles were sprinkled onto the carbon tape on the aluminum scanning electron microscope (SEM) sample stub. The sample was then coated with a 10 nm layer of platinum to improve conductivity and avoid surface charge accumulation. The SEM image was taken using an accelerating voltage of 10 kV and a secondary electron detector with a JEOL JSM 840A scanning electron microscope.

The microstructure of the sepiolite gel was imaged using cryo-SEM. To avoid hexagonal ice-crystal formation during cryo-freezing, the sample was subjected to a very high pressure and rapid freezing. A Leica EM PACT2 apparatus designed for this purpose was used. A minute sample of suspension was placed on two mini copper caps, each with a diameter of 1.5 mm and a depth of 0.2 mm. The cups were then pressed together before being placed in a loader for pressurization and rapid freezing in a liquid nitrogen bath. The sample was pressurized up to 2000 bar. A freezing rate as high as 25,000°C s^{-1} was employed. The frozen sample was then transferred to a Leica EM MED020 preparation system fitted with a Leica EM VCT100 control system, and sublimated at –100°C for 10 min before being coated with 8 nm of platinum. The sublimation time was optimized empirically to make sure that the frozen water from the exposed surface was removed, whilst the integrity of the microstructure was retained.

Studies have shown that hexagonal ice crystals will form on the cryo-SEM sample during the rapid freezing process at ambient pressure. These ice crystals distort the microstructure to a significant extent (Negre et al. 2004; Du et al. 2009, 2018; Leong et al. 2018). For comparison, the cryo-SEM images of sepiolite suspensions prepared at ambient pressure were also presented. The sepiolite suspensions in this case were mounted in two joined rivets before being plunged into liquid nitrogen for the freezing process, and the remaining processes were the same as used in the high-pressure freezing method.

The prepared samples for cryo-SEM were imaged at 5 kV with a Zeiss 55 field emission SEM fitted with a Leica EM VCT100 cryo and anticontamination system.

RESULTS AND DISCUSSION

Sepiolite Properties

The rheological properties of thixotropic clay gels are highly dependent on the morphology and charge properties of the particles (Du et al. 2018; Leong et al. 2018). The localization and location of the positive and negative charges giving rise to heterogeneous charge attraction and homogeneous charge repulsion are responsible for the complex rheological behavior displayed by these gels. A schematic model of the molecular and crystal structure of fibrous sepiolite (Fig. 1) shows the presence of open and pore channels (Ruiz-Hitzky 2011) and defines the direction of the three faces. The surface facing the *b* direction contained the –OH groups originating from the exposed side of the MgO octahedral sheets with pH-dependent charge. These –OH groups should remain positively charged at high pH of ~11 (Kosmulski 2009). The end of the fiber facing the *c* direction should also contain the pH dependent charged groups of the MgO sheet. The direction exposing the tetrahedral silica sheet surface is in the *a*- direction. The tetrahedral silica sheets possess the edge -Si-OH group which should be negatively charged at low pH, above 2. The chemical formula of the sepiolite

https://doi.org/10.1007/s42860-019-00050-z Published online by Cambridge University Press

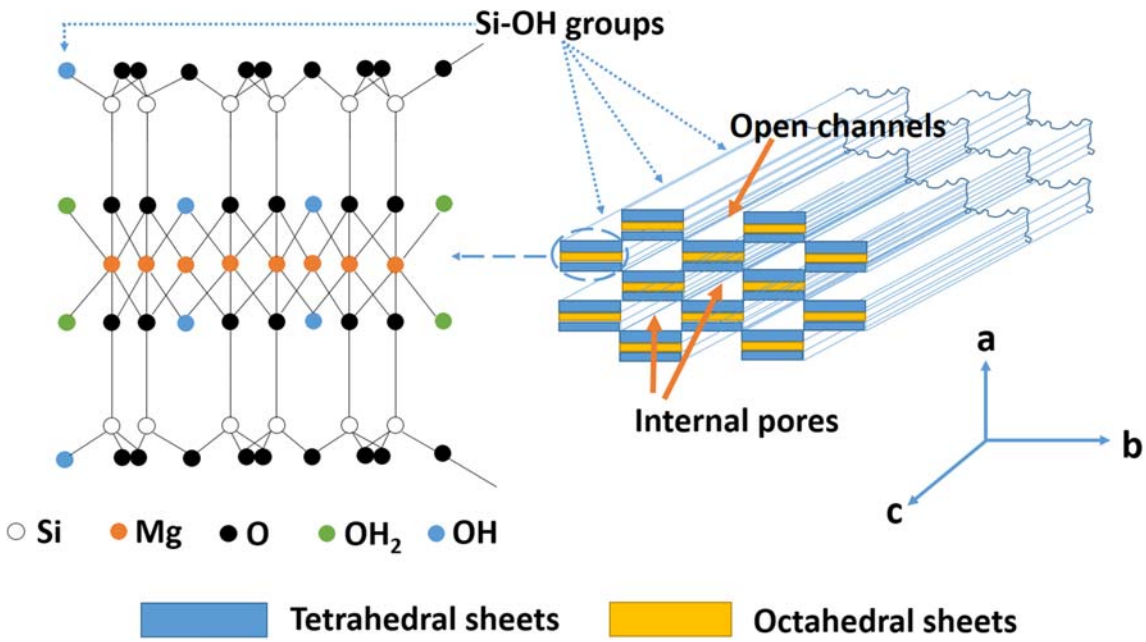

Fig. 1 A schematic model of sepiolite showing open channels and internal pores and molecular and crystalline structure (Ruiz-Hitzky 2011).

from Vallecas, Spain, was analyzed and found to be close to its theoretical value of $Mg_8Si_{12}O_{30}(OH)_4(OH_2)_4(H_2O)_8$ (Galan & Carretero 1999). Permanent charge due to isomorphic substitution should, therefore, be quite low in the SiO tetrahedral sheet.

Effect of Sonication Time

The SEM image (Fig. 2) showed that the as-received sepiolite powder was composed of large aggregates of fibrous materials. Loose fibers are seen clearly on the aggregate surface. As a suspension, this fibrous material must be well dispersed, i.e. these aggregates must be broken down into individual fibers. A high-intensity sonication method was employed for this purpose. The effect of sonication time on sepiolite dispersion was evaluated rheologically and via SEM imaging of samples of the dried suspensions obtained after various sonication times.

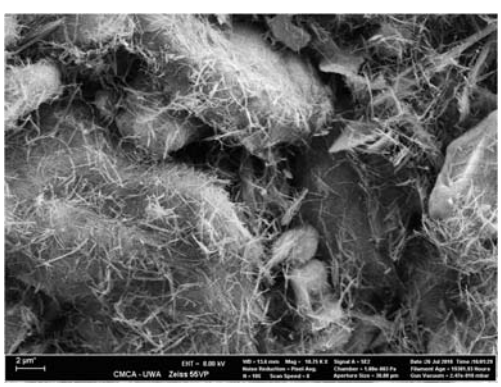

Fig. 2 SEM image of sepiolite particles.

Note that chemical methods for separating the fibers have been reported (Franchini et al. 2009).

The effect of sonication time on the yield stress of sepiolite suspensions (Fig. 3) was that the yield stress increased sharply during the first 3 min and then more gradually. Eventually, the increase stopped and the sonication time at which this occurs depended on the solids concentration. For the 2 and 3 wt.% sepiolite suspensions, the yield stress stopped increasing after 4 min of sonication. For the 5 wt.% suspension, 9 min was required.

Samples of the 5 wt.% suspension at various sonication times were collected and dried for SEM imaging. The images of samples subjected to sonication times of 0, 2, 6, and 10 min (Fig. 4) showed various degrees of dispersion. A high degree of dispersion was indicated by the absence of fiber agglomerates and bundles, and the extent of random fiber orientation. The image of the fiber suspension sonicated for 10 min showed a high degree of dispersion. The image of the sample at zero time showed the presence of large agglomerates. These large agglomerates disappeared upon sonication. However, the images of samples at sonication times of 2 and 6 min showed relatively large regions of fibers orientated in parallel configuration. The sample sonicated for 10 min showed that most fibers were orientated randomly. This is a reflection of a very high degree of fiber separation. An increasing degree of fiber separation can explain the increasing viscosity of sepiolite gel with (1) shear rate and (2) shearing time at a constant shear rate observed by Alvarez et al. (1984).

Yield stress is a measure of the strength of the microstructure in the suspension which depends on the particle and bond concentration forming the structure (Leong et al. 1993a, 1995). Individual sepiolite fibers were released with sonication time, thereby increasing the particle-number density. At the plateau

https://doi.org/10.1007/s42860-019-00050-z Published online by Cambridge University Press

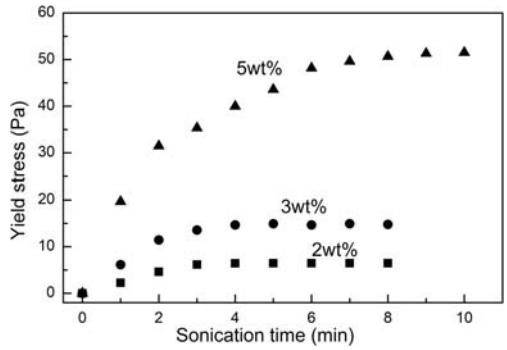

Fig. 3 The effect of sonication time on the yield stress of sepiolite suspensions.

yield stress region (Fig. 3), fiber separation and release became insignificant as the agglomerates were depleted.

Effect of Temperature

The effect of temperature on the yield stress of sepiolite suspension was also investigated. The suspension was kept at various constant temperatures in a water bath. Once the suspension reached a pre-set temperature, its yield stress was measured and its temperature was recorded with a thermometer immediately after the measurement. Before each yield-stress measurement, the suspension was stirred vigorously but briefly with a spatula. The yield stress increased with temperature (Fig. 5). The yield stress of a 3 wt.% sepiolite suspension increased from 10 to 22 Pa as the temperature increased from 10 to 70°C. Similar behavior was observed with synthetic hectorite gel (Shu et al. 2015). For Wyoming bentonite, the apparent viscosity of a 6 wt.% suspension aged at 21°C displayed a more complex relationship with temperature (Guven 1992b). This suspension displayed an initial decrease to a minimum value at 65°C, followed by a sharp increase with maximum viscosity observed at 85°C. The Hamaker constant of the sepiolite in water should also increase with temperature (Israelachvili 2011) and this may play a role in the yield-stress increase.

Effect of pH, Ionic Strength, and TSPP

The effect of pH on the yield-stress behavior of 2, 3, and 5 wt.% sepiolite suspensions was recorded as pH was reduced from 12 to 2 (Fig. 6). All three suspensions were dispersed completely at pH >11, manifested by a zero yield stress. The yield stress increased from zero at pH 11 to a maximum value at pH 8, which remained constant in the 8–4 pH range. This stress increased with solids concentration: 8, 35, and 60 Pa for the 2, 3, and 5 wt.% suspensions. A greater particle concentration should lead to the formation of a stronger microstructure. The yield stress was lower at pH <4. Clay is known to become more soluble at low pH and this may be responsible for the lower yield stress at pH <4 (Simonton et al. 1988). A similar yield stress-pH behavior for palygorskite gel was reported in terms of

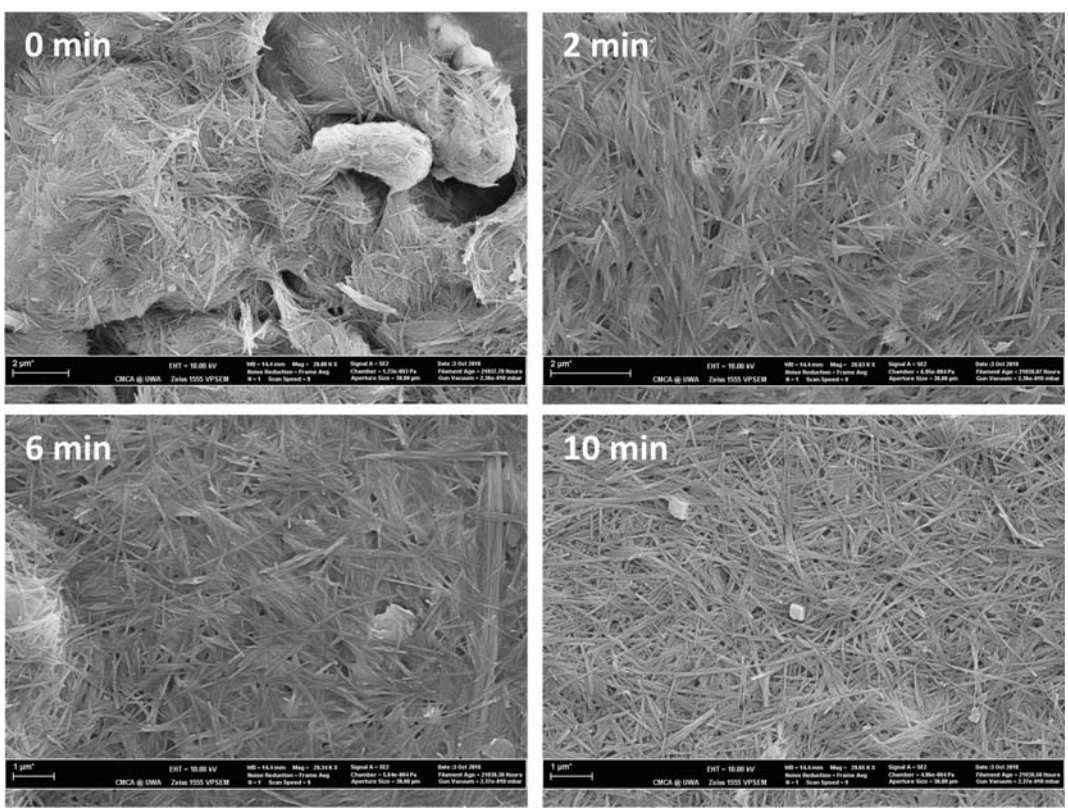

Fig. 4 SEM images showing the effect of sonication time on fiber separation. The more random the fiber orientation, the higher the degree of fiber separation.

https://doi.org/10.1007/s42860-019-00050-z Published online by Cambridge University Press

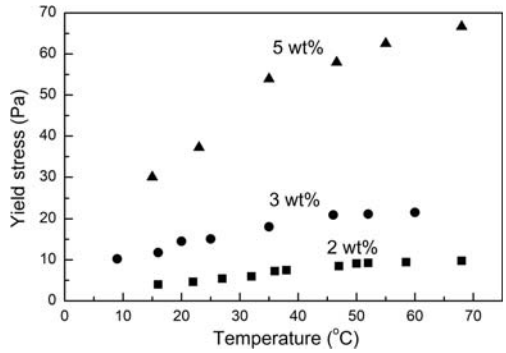

Fig. 5 The effect of temperature on the yield stress of sepiolite suspensions.

Bingham yield stress (Neaman & Singer 2000). For the palygorskite gel with low ionic strength, zero yield stress was observed at pH >9. The constant maximum yield stress was located between pH 2 and 7.

A similar viscosity-pH behavior was also reported for thixotropic suspensions of brown sepiolite from Turkey (Çınara et al. 2009). The viscosity was very low at pH 11 and increased sharply to a maximum value at pH 8. The viscosity then decreased gradually with decreasing pH.

Ionic strength produced various effects on the yield stress of 5 wt.% sepiolite suspensions (Fig. 7) depending on the pH. The salt concentration evaluated ranged from 0 (deionized water) to 1 M KCl. Ionic strength had no significant effect on the yield stress at pH <8. The insensitivity of sepiolite suspensions to salt concentration is, therefore, only true at pH <8. The effect of ionic strength was quite pronounced at pH >8. The yield stress increased with ionic strength more sharply at higher pH such as 12. The yield-stress behavior was displayed over a broader pH range; e.g. the gels with 0.1 and 1 M KCl registered significant yield stress at pH ~13. The maximum yield stress was then located at a higher pH of ~9.5. This yield stress was much higher for the gels with 0.1 and 1 M KCl than for those prepared with DI water. These two high-salt gels displayed the same maximum yield stress of 90 Pa, 1.5 times larger than that (60 Pa) prepared in DI water. The broadening of the yield-stress behavior from pH 8 to 13 with increasing ionic strength is a classic behavior displayed by suspensions in which the EDL repulsive and van der Waals attractive forces play a significant role in determining the nature and strength of the net interparticle force (Leong et al. 1993b). This behavior is normally associated with the pH-dependent charge playing a prominent role in determining the strength of the EDL force at a fixed salt concentration. Zeta potential data presented later will be used to explain the yield-stress state of some of these suspensions.

The zero yield stress located at pH > 11 (Fig. 6) is a manifestation of the sepiolite fibers interacting repulsively via the EDL force. For the EDL force to dominate the interaction, the fibers must have acquired a sufficient negative charge (Guven 1992a). The net increase will be shown to be due to the simultaneous decrease in the positive charge density and increase in the negative charge density. At high ionic strength, the EDL is compressed, shielding the surface charge. As a result, the fibers can come close enough together for the van der Waals attractive force to dominate the interactions (Sabah et al. 2007). A network structure is then formed and the yield stress is a measure of the strength of this structure. The yield stress at pH > 11 for the high ionic strength gels (Fig. 7) was due to this van der Waals force. The increasing yield stress with ionic strength at any pH above 8 was due to the strengthening of the fiber–fiber bond by a net attractive force increasing in strength, i.e. the van der Waals force minus a diminishing EDL force. The insensitivity of the yield stress to pH and ionic strength at pH between 4 and 8 is quite mysterious. Heterogeneous charge attraction forming the fiber–fiber bond if present should be important in this pH range.

Zeta potential is a measure of the strength of the repulsive force and its sign is an indication of the type of the net charge. The zeta potential-pH behavior of the pristine sepiolite suspension (Fig. 8a) showed the presence of a point of zero zeta potential or zero net charge located at pH ~3.3. Kosmulski

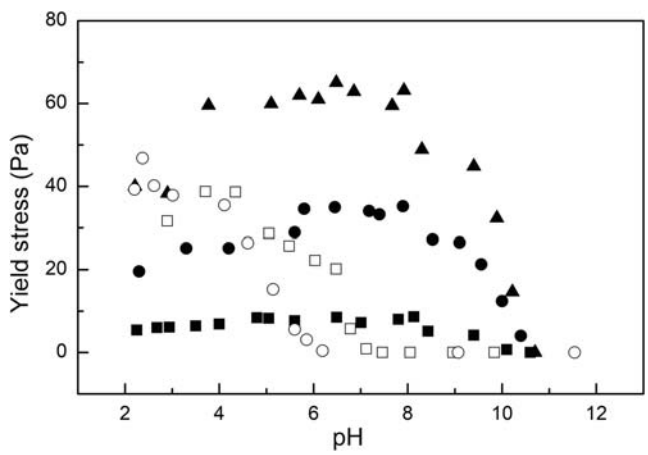

Fig. 6 The effect of pH on the yield stress of sepiolite suspensions: ■, 2 wt.% sepiolite suspension; ●, 3 wt.%; ▲, 5 wt.%; □, 5 wt.% with 2 dwb% TSPP; ○, 5 wt.% with 6 dwb% TSPP.

https://doi.org/10.1007/s42860-019-00050-z Published online by Cambridge University Press

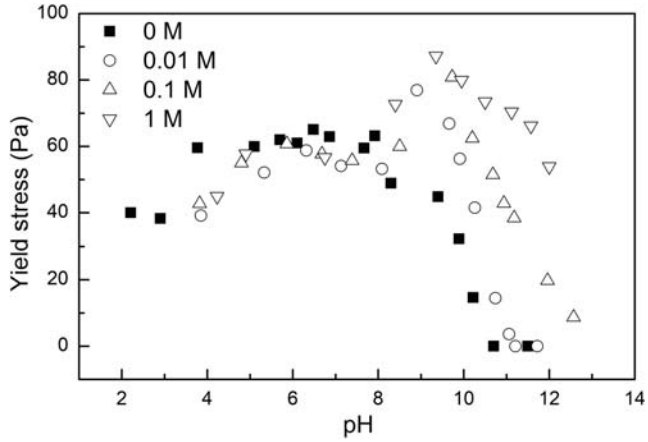

Fig. 7 Effect of ionic strength or KCl salt concentration on the yield stress of sepiolite suspensions.

(2018) reported that most clay minerals displayed an isoelectric point (IEP) in the pH range of 2 to 4. This sepiolite is net negatively charged over a wide pH range of 3–12, as reflected by the zeta potential being negative in this pH range. The zeta potential decreased from zero at pH 3 to –49 mV at pH 12. An earlier measurement (Fig. 8b) showed a similar result with the zeta potential decreasing from –6 mV at pH 4 to –43 mV at pH 12. A similar IEP of 3.7 was reported for a sepiolite (Pangel S15) with a composition similar to that of Pangel S9 (Sabah et al. 2007). A sepiolite sourced from Hebei, China, displayed a similar IEP of 4 but it displayed a relatively small negative zeta potential of –22 mV at pH 12 (Zhang et al. 2018). A similarly low-magnitude zeta potential of –22 to –18 mV was observed for a Turkish sepiolite which, however, displayed a higher IEP of 6.5 (Alkan et al. 2005). The zeta potential (Fig. 8a) showed small changes in value in the pH range of 4 to 8, from –9 to –12 mV, and this corresponded to the pH and ionic strength insensitive yield-stress region. The onset of zero yield stress at pH ~ 10.5 corresponded to a zeta potential of –30 mV. The increasing magnitude of the zeta potential at pH > 8 correlated well with the trend of a decreasing yield stress with pH (Fig. 6).

The maximum yield stress in the pH range 4 to 8 corresponded to a zeta potential of ~–10 mV. This suggests the presence of (1) a relatively weak EDL repulsive force and (2) another attractive force in addition to the van der Waals force. In most clays, this attractive force is the positive-negative charge attraction. The zeta potential of sepiolite treated with TSPP should confirm the presence of positive charge sites. This insensitivity of the yield stress to ionic strength at pH = 4–8, suggested that (1) the EDL repulsive force was insignificant and (2) the strength of the heterogeneous charge attraction at fiber–fiber contact was not dependent on ionic strength.

Polyphosphate additives are known peptizers for clay slurries (Bergaya & Lagaly 2006). These additives can have as many as 20–30 negative charges per molecule depending on the degree of polymerization. Upon adsorption, they neutralize the positive edge charges, thus increasing the negative charge density of the clay particles. TSPP has a significant effect on the yield stress and the zeta potential of sepiolite suspensions (Figs 6 and 8b). TSPP increased the magnitude of the negative zeta potential, shifted the onset of the zero yield-stress region to a lower

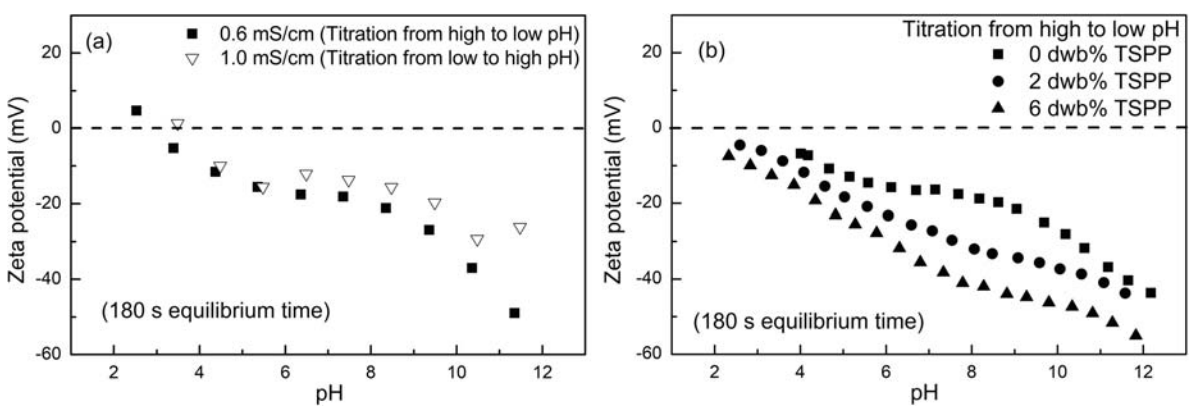

Fig. 8 The effect of pH on the zeta potential of sepiolite suspensions: (**a**) without TSPP and (**b**) with TSPP additives. Pangel S9 displayed an isoelectric point at pH 3 when potentiometrically titrated from high to low pH and at pH 3.7 when titrated in the reverse direction.

https://doi.org/10.1007/s42860-019-00050-z Published online by Cambridge University Press

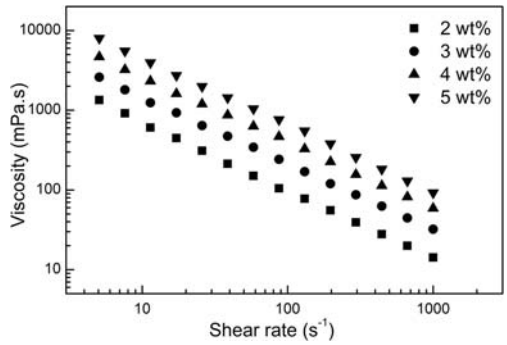

Fig. 9 The flow behavior of sepiolite suspensions

pH, decreased the maximum yield stress, and shifted it to a lower pH. The pH region for the zero yield stress is now located at pH > 6 for suspensions treated with 6 dwb% TSPP and pH > 7 for those treated with 2 dwb% TSPP. The maximum yield stress of these two treated suspensions was reduced by 20 Pa to ~40 Pa and located at pH <4. Between pH 2 and 4, the yield stress appeared to be constant.

The magnitude of the negative zeta potential increased with TSPP concentration. This is a strong indication that sepiolite possesses positive charge sites to adsorb the TSPP. The location of these charge sites and the manner in which they interact attractively with the negative charge sites of other fibers will be explored in a subsequent section. Adsorbed TSPP enhanced the EDL repulsive force between the fibers. As a result, this force dominated the fiber–fiber interaction at a lower pH, as reflected by the shifted of the onset of the zero yield stress. The onset of the zero yield stress also corresponded to a zeta potential of –30 mV.

The Flow Behavior of Sepiolite Suspensions

The viscosity-shear rate behavior of sepiolite suspensions with concentration ranging from 2 to 5 wt.% (Fig. 9) showed pronounced shear-thinning behavior in the 5 to 1000 s^{-1} shear rate range. The decrease in the viscosity with shear rate was linear on a log-log scale at all solid loadings. The linear relationship is a classic example of a power law flow behavior. In terms of viscosity, the power law model is given by:

$$\mu = K\dot{\gamma}^{n-1} \quad (1)$$

where μ is the viscosity; K, the consistency index; $\dot{\gamma}$, the shear rate; and n, the power index. The slope of the linear relationship between μ and $\dot{\gamma}$ plotted on a log scale is n–1. The power law index (Table 1) was 0.15±0.01, 0.17±0.01, 0.18±0.01, and 0.16±0.01 for the sepiolite suspensions with 2, 3, 4, and 5 wt.% solids. The power law indexes were numerically very close to each other so the power law index could be regarded as independent of solid loading. Its corresponding consistency index K (Table 1) was $5.0\pm0.1\times10^3$, $10.0\pm0.3\times10^3$, $17.4\pm0.4\times10^3$, and $31.6\pm0.7\times10^3$. The shear thinning behavior was attributed to an increasing degree of fiber bond breakage and alignment with shear rates. At pH >9, the viscosity decreased sharply with pH and the rheological behavior became Newtonian (data not shown).

The Ageing Behavior

The freshly prepared suspensions were left at rest for a few days to allow surface charging, ion transport, and hydration to reach the SCE state. The SCE state was determined by yield stress (measured immediately after the suspension was agitated or sheared) becoming independent of time since preparation (Fig. 10). The sepiolite suspensions reached the SCE state almost immediately after preparation.

A unique feature of 2:1 platy clay minerals is the localization of the different types of surface charge, i.e. the pH-dependent charge on the edge of the octahedral sheet of alumina or magnesia and the permanent negative charge on the tetrahedral silica face. These localized heterogeneous charges cause the clay particles in suspension to experience both repulsive (EDL) and attractive (positive-negative charge) forces at the same time. These forces caused the platelet clay particles to form a 3-D network structure in suspension at very dilute concentration of a few percent solids. Another important contributing factor is the nano-size of the clay particles (Du et al. 2018; Leong et al. 2018). This structure should break down upon shearing. For a thixotropic clay gel this structure recovered with time, if undisturbed. Structural recovery is usually reflected by the yield stress increasing with ageing time. The 3-D network structure formation and heterogeneous charge fiber interaction of the thixotropic sepiolite gel are next to be examined for comparison with that obtained for the platy 2:1 clay mineral gels.

Pre-sheared sepiolite suspensions were found to display similar time-dependent behavior. Increasing yield stress with ageing time was observed for sepiolite suspensions with concentration ranging from 2 to 5 wt.% solids (Fig. 11). The yield stress continued to increase after 10,000 min (~7 days). The structural recovery process was, thus, very long. Depending on the solids loading, the time for the structure to recover fully was between 6 and 70 days. The dilute suspensions took less time. The yield

Table 1 The power law parameters for the flow behavior of sepiolite suspensions.

Solid concentration (wt.%)	2	3	4	5
n^a	0.15±0.01	0.17±0.01	0.18±0.01	0.16±0.01
K^a	$5.0\pm0.1\times10^3$	$10.0\pm0.3\times10^3$	$17.4\pm0.4\times10^3$	$31.6\pm0.7\times10^3$
Adjusted R^2	0.99	0.99	0.99	0.99

a: Data reported with standard error

https://doi.org/10.1007/s42860-019-00050-z Published online by Cambridge University Press

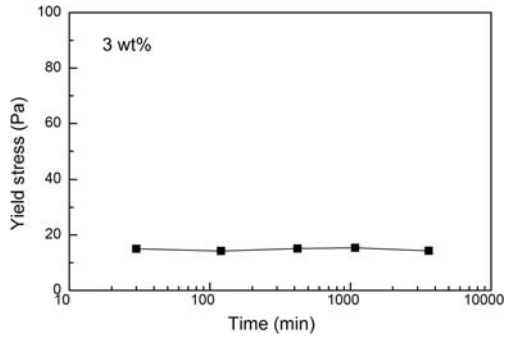

Fig. 10 The determination of the surface chemical equilibrium state. The yield stress was measured immediately after vigorous stirring or shearing of the suspension.

stress of the fully aged suspensions was 3–5 times larger than the initial yield stress. Most of the increase in yield stress occurred in the first two weeks of ageing. The yield stress reached >80% of the fully recovered state yield stress during this period. Note that the error bar of the yield stress data is smaller than the size of the legend (Fig. 11).

An ageing model, the Leong model based on Smoluchowski rate theory and second-order aggregation kinetics (de Kretser & Boger 2001), is commonly used to describe the long-time ageing behavior of clay gels (Chang & Leong 2014; Sehly et al. 2015; Leong et al. 2018). It is a three-parameter model given by (de Kretser & Boger 2001; Yoon & el Mohtar 2013):

$$\tau_y(t) = \tau_{y\infty}\left(1-\frac{1-\left(\frac{\tau_{y0}}{\tau_{y\infty}}\right)^{3/2}}{1+K_r t}\right)^{2/3} \quad (2)$$

where $\tau_y(t)$ is the time-dependent yield stress; τ_{y0}, the initial yield stress measured at 0 min; $\tau_{y\infty}$, the yield stress at complete structural recovery; and K_r, the inverse of the Leong model time constant.

With τ_{y0} and $\tau_{y\infty}$ known, only the parameter K_r of the Leong model is unknown. The model was reorganized into a linear relationship:

$$\frac{\left(1-\left(\frac{\tau_{y0}}{\tau_{y\infty}}\right)^{1.5}\right)}{\left(1-\left(\frac{\tau_{y(t)}}{\tau_{y\infty}}\right)^{1.5}\right)} = K_r{}^{*}t + 1 \quad (3)$$

or:

$$y = mx + c \quad (4)$$

with $m = K_r$, c should be 1 according to the model.

A linear regression fit of the experimentally determined x-y data set was applied to obtain the m or K_r value. Note that the error was very large at yield stress $\tau_y(t)$ close to the equilibrium yield stress $\tau_{y\infty}$ value at long ageing time due to the denominator being very small – the product of the difference between two values with the variable being close to 1. The c value (Table 2) was indeed close to 1 for all four sepiolite concentrations. The standard error provided by the linear regression result is included in Table 2.

The linear regression fitting of the ageing data to obtain K_r of the Leong model (Table 2) produced fits with correlation (R^2) values ranging from 0.92 to 0.97. The Leong model fit to the experimental data (Fig. 11) performed generally well for the suspensions with 3, 4, and 5 wt.% solids. The time constant, $1/K_r$, was determined to be $1.4\pm0.2\times10^3$, $1.8\pm0.2\times10^3$, $3.0\pm0.4\times10^3$, and $3.1\pm0.3\times10^3$ min for the 2, 3, 4, and 5 wt.% suspensions, respectively. Another method of looking at the effect of fiber concentration on the structural reformation kinetics is to compare the time taken to reach a given multiple of the measured yield stress at zero ageing time. The time taken to reach three times the measured yield stress at zero ageing time was observed to increase with fiber concentration, viz., 1300, 11,300, 19,300, and 22,100 min for the 2, 3, 4, and 5 wt.% suspensions, respectively. For the time taken to increase the yield stress by a factor of two, the trend is the same: 190 min for 2 wt.% and much longer times at high concentration. These

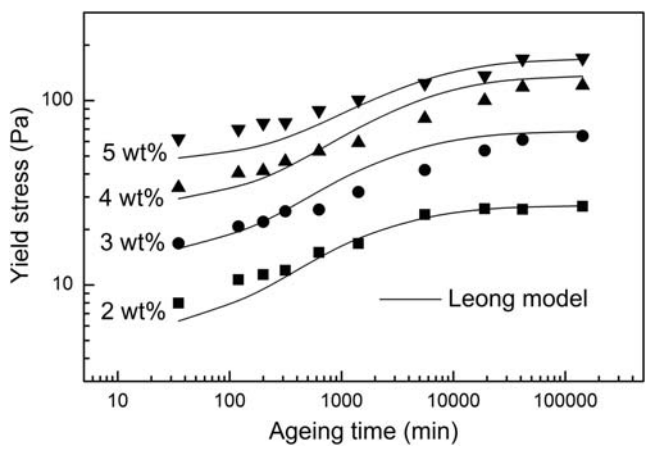

Fig. 11 The ageing behavior of sepiolite suspensions. Symbols ■●▲▼: experimental data; Line: Leong model with parameters as in Table 2.

https://doi.org/10.1007/s42860-019-00050-z Published online by Cambridge University Press

Table 2 The Leong model parameters obtained by linear regression using *Origin* software.

Solid concentration (wt.%)	2	3	4	5
τ_{y0} (Pa)	5.5	14.1	27.3	46.8
$\tau_{y\infty}$ (Pa)	27.0	68.5	137.0	169.5
$(1/K_r)^a$ (min)	$1.4\pm0.2\times10^3$	$1.8\pm0.2\times10^3$	$3.0\pm0.4\times10^3$	$3.1\pm0.3\times10^3$
c^a	1.05±0.03	1.01±0.01	1.03±0.01	1.09±0.02
Adjusted R^2	0.94	0.96	0.92	0.97

a: Data reported with standard error

longer times are quite similar for the 3 to 5 wt.% solids, 840 to 970 min. The high-fiber concentration slows the kinetics of reaching the structural state of minimum free energy.

A 4 wt.% sepiolite suspension was prepared, employing only 3 min of sonication instead of 10 min to show the effect of fiber separation on the ageing behavior of the suspension (Fig. 12). The yield stress was lower compared to the same solids suspension shown in Fig. 11. Despite a lower degree of fiber separation, the suspension still displayed time-dependent behavior. The yield stress continued to increase even after 3 weeks of ageing. The result also showed good reproducibility of the ageing result. In the first ageing cycle, the pre-sheared suspension was aged for 18 days (solid square symbol) and then sheared again for the second ageing cycle (open circle). This cycle lasted for 21 days. Excellent reproducibility was observed in the first 10 days.

The Gel Microstructure

SEM images (Fig. 13) revealed the microstructure of the 5 wt.% sepiolite suspension with an equivalent KCl concentration of ~0.001 M. The SEM images also showed, at various magnifications, the microstructure of the sample prepared at high pressure (~2000 bar) and rapid freezing (Fig. 13a, b, c). In these images the fibers are long and straight and appear very rigid. The colloidal nature of these fibers is reflected by its diameter being much smaller than 200 nm. The length is certainly >1 μm. The ice-affected microstructure formed by plunge freezing at atmospheric pressure can be seen in Fig. 13d (Norrish & Rausell-Colom 1962). The hexagonal ice formed in the process pushed the fibers together to form large, thick sheets. Some of these sheets were >10 μm long. A SEM image of a critical-point dried gel sample from the same clay deposit (Vallecas) did not show the same microstructure (Simonton et al. 1988). Regions of high-fiber aggregation were present and individual fibers were rarely seen. Critical point drying was employed to eliminate surface tension forces during air drying and is supposed to preserve the gel microstructure (Anderson 1951). The alcohol treatment could have affected the fiber interaction configuration and hence the microstructure.

The low-magnification image (Fig. 13a) showed a high concentration of fibers organized in a random fashion. The higher-magnification images (Fig. 13b and c) showed fibers interacting in the cross configuration, in which one fiber can interact with several fibers. The crossing point between the interacting fibers or rods was located at any point along the length of the sepiolite particles. Some of the crossing points were near the end of the fiber. The angle of the cross fibers varied. Some were interacting close to 90° but most were at less than 90°. This attractive crossing interaction configuration was responsible for the 3-D connected microstructure and the yield stress of the gel. A perfect parallel interaction configuration was not seen in these images, but a non-perfect parallel configuration was observed. The fibers interacting in this configuration showed a finite separation distance, suggesting a strong repulsive interaction. The concentration of the cross-fiber interaction was relatively low. This suggests that only specific orientations of the faces of the fibers give rise to

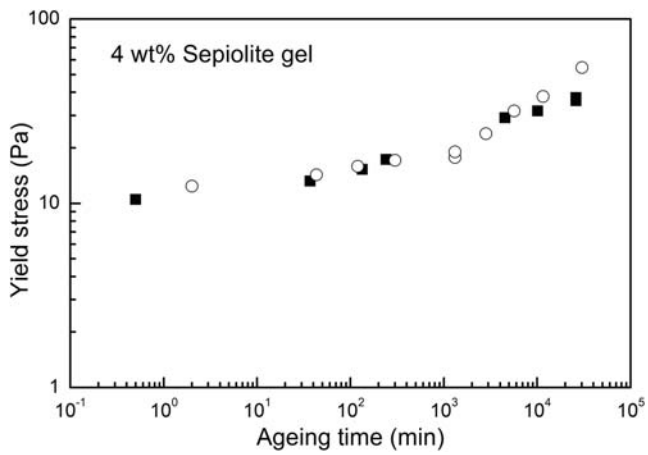

Fig. 12 Ageing behavior of sepiolite suspension sonicated for 3 min and its reproducibility.

https://doi.org/10.1007/s42860-019-00050-z Published online by Cambridge University Press

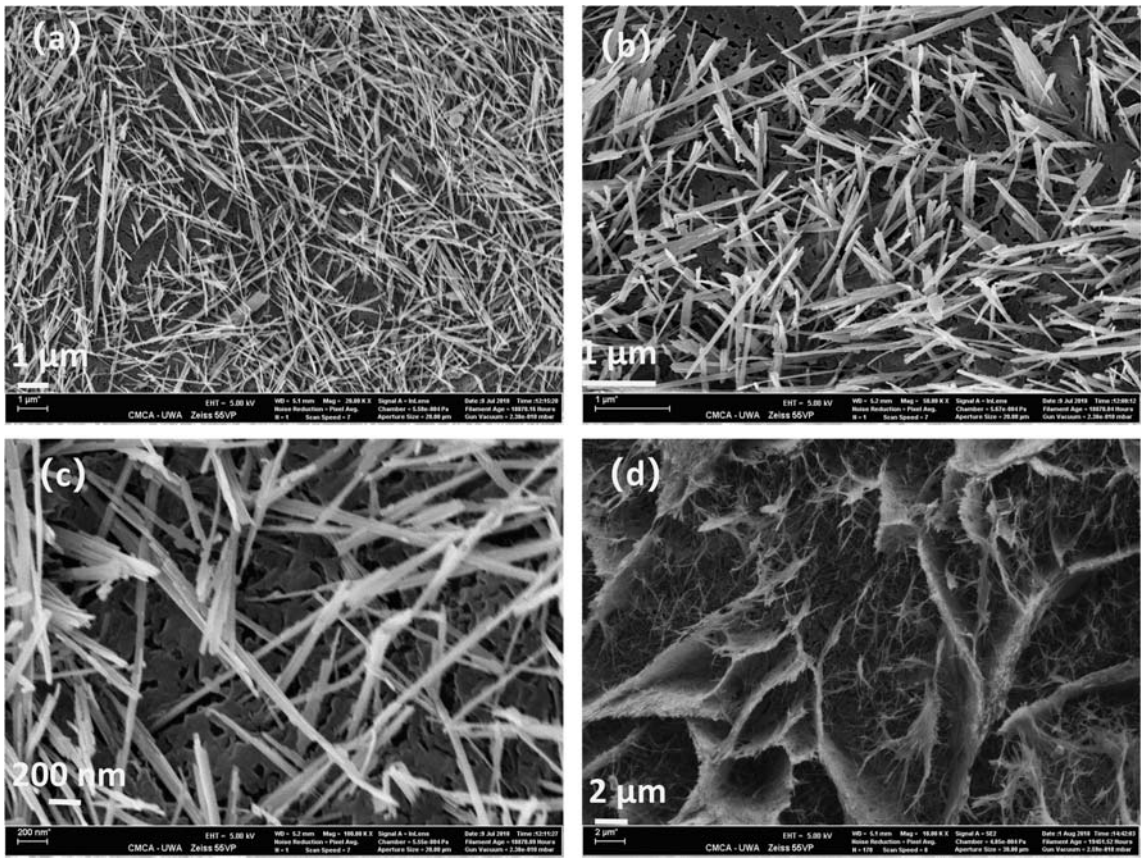

Fig. 13 The microstructure of 5 wt.% sepiolite suspension: (**a**) high-pressure freezing – 20× magnification; (**b**) high-pressure freezing – 50× magnification; (**c**) high-pressure freezing – 100× magnification; (**d**) plunge freezing (ice-affected structure).

attractive interaction. Impurities, which are usually irregular in shape, appeared to be absent from the microstructure. This was also observed in the microstructure of bentonite gel (Du et al. 2019) and as-received hectorite (SCHa-1) gel with 50 wt.% impurities (Au et al. 2019). The relationship between maximum yield stress and hectorite content was the same for purified and unpurified hectorite gel. Hectorite was, therefore, the only active ingredient controlling the rheological property of the gel that did interact with impurities in any significant manner.

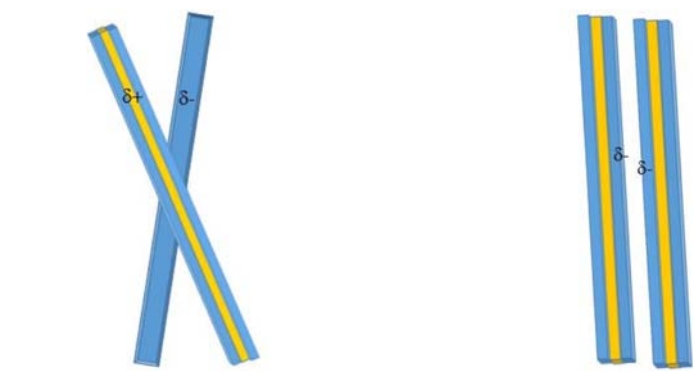

Fig. 14 A schematic diagram showing (**a**) attractive and (**b**) repulsive surface–surface interactions of sepiolite fibers. Only one structural SiO_2-MgO-SiO_2 element of the surface showing the nature of the net surface charge was used to illustrate the attractive and repulsive interaction.

https://doi.org/10.1007/s42860-019-00050-z Published online by Cambridge University Press

The fiber–fiber bond in the cross configuration should be formed by heterogeneous charge and van der Waals attraction (Fig. 14a). This should occur between the faces of the fibers in the *b* and *a* directions. Heterogeneous charge attraction can occur between the positive charge of the surface –Mg-OH and the permanent negative charge of the tetrahedral SiO_2 layer or the negative charge of the edge –Si-OH groups. Attractive interaction in the parallel configuration between fibers in the *b* and *a* directions was not observed either. This suggests that the repulsive force dominates the interaction. The end–face interaction between fibers in the *c* and *a* directions was not observed either. Evidence indicating the participation of the edge –Si-OH group in attractive fiber–fiber interactions was reported by Aznar et al. (1992). The peptization of the sepiolite gel by methylene blue was presented as the evidence. The positively charged methylene blue adsorbed and neutralized the negative charge of the –Si-OH group.

Repulsive interaction should occur between the negatively charged silica faces of the fibers (in the *a* direction) whether in the cross or parallel configuration (Fig. 14b). This repulsive interaction was responsible for keeping the fibers apart and opening up the network structure. The thixotropic behavior occurring at very dilute concentration (2 wt.% suspension) is a reflection of this very open network structure in this gel. Each fiber experienced both attractive and repulsive forces from interactions with its nearest neighbors. During the initial state of ageing, all fibers in the network experienced a net force. These fibers will have to move or orient to attain a state of force balance involving some degree of bond breakage and formation. This process takes a long time, which was reflected in the long time scale of the ageing behavior. This fiber movement or orientation should stop when the zero net force equilibrium state is attained. At this state, the global free energy of this microstructure should be zero. AFM characterization of the fiber–fiber interactions (Mizuno et al. 2010) is an ideal way of establishing the presence of repulsive and attractive interactions in the face-face cross-fiber configuration. Multiple fiber pair interactions may be needed to show in a statistically significant manner that both repulsive and attraction interactions are present, as identifying the *a* and *b* direction faces is not possible. A new technique for mounting 100 nm diameter fibers for such characterization may need to be developed.

CONCLUSIONS

For a high degree of fiber separation, a sonication time of 10 min with a high-intensity sonic probe is required. The yield stress also increased with increasing degree of fiber separation, solids concentration, and temperature. These suspensions displayed highly shear-thinning flow behavior.

The pH has a significant effect on the yield stress only at pH >8. The maximum yield stress located at pH ~8 decreased to zero at pH 11. TSPP additive shifts the pH at the onset of zero yield stress to a lower pH; 6 at 6 dwb% TSPP and 7 at 2 dwb% TSPP. With or without TSPP, the onset of zero yield stress occurred at the zeta potential of –30 mV.

Sepiolite suspension is insensitive to ionic strength or salt concentration (up to 1 M KCl) only at pH< 8. At pH >8, the yield stress increased with ionic strength.

Sepiolite suspensions displayed ageing behavior with a long timescale. The yield stress increased with ageing time over a period of several days. The Leong model described the long time scale ageing behavior well.

The microstructure of sepiolite suspensions showed random orientation of the fibers. Attraction interaction between the fibers occurred in the cross-configuration. The angle of this cross interaction ranged from small to 90°. Attraction should be between the negative silica face and the face with the exposed edge of the MgO octahedral sheet containing the pH-dependent positive charge. All fibers in the network experienced both attractive and repulsive interactions. Initially, they all experience a net force. In response, they move, orientate, or adjust continually so as to attain a force equilibrium or a zero net force state. This process takes a long time and is responsible for the long-time ageing behavior.

ACKNOWLEDGMENTS

Pengfei Liu thanks the Australian Research Training Program (RTP) for providing the financial support for the PhD study. The authors acknowledge the technical assistance of Lyn Kirilak and use of the facilities of Microscopy Australia at the Centre for Microscopy, Characterisation & Analysis, The University of Western Australia, a facility funded by the University and State and Commonwealth Governments. Special thanks to Dr Xuhao Du and Mr Marty Firth for their help in model fitting and error analysis. The authors also wish to thank the reviewers and editors for making this a better paper.

Compliance with ethical standards

Conflict of interest

The authors declare that they have no conflict of interest.

REFERENCES

Alkan, M., Demirbaş, Ö., & Doğan, M. (2005). Electrokinetic properties of sepiolite suspensions in different electrolyte media. *Journal of Colloid and Interface Science, 281*, 240–248.

Alvarez, A., Singer, A., & Galan, E. (1984). Sepiolite: properties and uses. *Developments in Sedimentology, 34*, 253–287.

Anderson, T. F. (1951). Techniques for the preservation of three-dimensional structure in preparing specimens for the electron microscope. *Transactions of the New York Academy of Science, 13*, 130–134.

Au, P. I., Du, M. Y., Liu, J. S., Bashirul Haq, M., & Leong, Y. K. (2019). Surface chemistry, rheology and microstructure of as-received SHCa-1 hectorite gels. *Clay Minerals, 54*, 269–275.

Aznar, A. J., Casal, B., Ruiz-Hitzky, E., Lopez-Arbeloa, I., Lopez-Arbeloa, F., Santaren, J., & Alvarez, A. (1992). Adsorption of methylene blue on sepiolite gels: spectroscopic and rheological studies. *Clay Minerals, 27*, 101–108.

Bergaya, F., & Lagaly, G. (2006). General introduction: clays, clay minerals, and clay science. In F. Bergaya, B. K. G. Theng, & G. Lagaly (Eds.), *Handbook of Clay Science: Developments in Clay Science* (Vol. 1, pp. 1–18). Amsterdam: Elsevier.

https://doi.org/10.1007/s42860-019-00050-z Published online by Cambridge University Press

Borgnino, L. (2013). Experimental determination of the colloidal stability of Fe(III)-montmorillonite: effects of organic matter, ionic strength and pH conditions. *Colloids and Surfaces A: Physicochemical Engineering Aspects, 423*, 178–187.

Bounoua, S., Lemaire, E., Férec, J., Ausias, G., & Kuzhir, P. (2016). Shear-thinning in concentrated rigid fiber suspensions: Aggregation induced by adhesive interactions. *Journal of Rheology, 60*, 1279–1300.

Castro-Smirnov, F. A., Ayache, J., Bertrand, J.-R., Dardillac, E., Le Cam, E., Piétrement, O., Aranda, P., Ruiz-Hitzky, E., & Lopez, B. S. (2017). Cellular uptake pathways of sepiolite nanofibers and DNA transfection improvement. *Scientific Reports, 7*, 5586.

Chang, W. Z., & Leong, Y. K. (2014). Ageing and collapse of bentonite gels—effects of Li, Na, K and Cs ions. *Rheologica Acta, 53*, 109–122.

Çınara, M., Can, M. F., Sabah, E., Karagüzel, C., & Çelik, M. S. (2009). Rheological properties of sepiolite ground in acid and alkaline media. *Applied Clay Science, 42*, 422–426.

de Kretser, R. G., & Boger, D. V. (2001). A structural model for the time-dependent recovery of mineral dispersions. *Rheologica. Acta, 40*, 582–590.

Dijkstra, M., Hansen, J. P., & Madden, P. A. (1997). Statistical model for the structure and gelation of smectite clay. *Physical Review E, 55*, 3044–3053.

Djalili-Moghaddam, M., & Toll, S. (2005). A model for short-range interactions in fiber suspensions. *Journal of Non-Newtonian Mechanics, 132*, 73–83.

Du, J., Pushkarova, R. A., & Smart, R. S. C. (2009). A cryo-SEM study of aggregate and floc structure changes during clay settling and raking processes. *International Journal of Minerals Processing, 93*, 66–72.

Du, M., Liu, J., Clode, P. L., & Leong, Y. K. (2018). Surface chemistry, rheology and microstructure of purified natural and synthetic hectorite suspensions. *Physical Chemistry Chemical Physics, 20*, 19221–19233.

Du, M., Liu, J., Clode, P. L., & Leong, Y. K. (2019). Microstructure and rheology of bentonite slurries containing multiple-charge phosphate-based additives. *Applied Clay Science, 169*, 120–128.

Franchini, E., Galy, J., & Gérard, J.-F. (2009). Sepiolite-based epoxy nanocomposites: relation between processing, rheology, and morphology. *Journal of Colloid and Interface Science, 329*, 38–47.

Galan, E. (1996). Properties and applications of palygorskite-sepiolite clays. *Clay Minerals, 31*, 443–453.

Galan, E., & Carretero, M. I. (1999). A new approach to compositional limits for sepiolite and palygorskite. *Clays and Clay Minerals, 47*, 399–409.

Guven, N. (1992a). Molecular aspects of aqueous smectite suspensions. In N. Guven & M. Pollastro (Eds.), *CMS Workshop Lectures, Vol. 4, Clay-water Interface and its Rheological Implications* (pp. 1–80). Boulder, Colorado, USA: The Clay Minerals Society.

Guven, N. (1992b). Rheological aspects of aqueous smectite suspensions. In N. Guven & M. Pollastro (Eds.), *CMS Workshop Lectures, Vol. 4, Clay-water Interface and its Rheological Implications* (pp. 81–126). Boulder, Colorado, USA: The Clay Minerals Society.

Israelachvili, J. N. (2011). *Intermolecular and Surface Forces*. London: Academic press.

Johnson, S. B., Franks, G. V., Scales, P. J., Boger, D. V., & Healy, T. W. (2000). Surface chemistry–rheology relationships in concentrated mineral suspensions. *International Journal of Minerals Processing, 58*, 267–304.

Joshi, Y. M., Reddy, G. R. K., Kulkarni, A. J., Kumar, N., & Chhabra, R. P. (2008). Rheological behavior of aqueous suspensions of laponite: new insights into the ageing phenomena. *Proceedings of the Royal Society A: Mathematical, Physical and Engineering Sciences, 464*, 469–489.

Kosmulski, M. (2009). Compilation of PZC and IEP of sparingly soluble metal oxides and hydroxides from literature. *Advances in Colloid and Interface Science, 152*, 14–25.

Kosmulski, M. (2018). The pH dependent surface charging and points of zero charge. VII. update. *Advances in Colloid and Interface Science, 251*, 115–138.

Larson, R. G. (1999). *The Structure and Rheology of Complex Fluids*. New York: Oxford University Press.

Leong, Y. K., & Ong, B. C. (2015). Polyelectrolyte-mediated interparticle forces in aqueous suspensions: molecular structure and surface forces relationship. *Chemical Engineering Research and Design, 101*, 44–55.

Leong, Y. K., Scales, P. J., Healy, T. W., Boger, D. V., & Buscall, R. (1993a). Rheological evidence of adsorbate mediated short range steric forces in concentrated dispersions. *Journal of the Chemical Society, Faraday Transaction, 89*, 2473–2478.

Leong, Y. K., Katiforis, N., Harding, D. B. O.' C., Healy, T. W., & Boger, D. V. (1993b). Role of rheology in colloidal processing of ZrO_2. *Journal of Material Processing & Manufacturing Science, 1*, 445–453.

Leong, Y. K., Scales, P. J., Healy, T. W., & Boger, D. V. (1995). Interparticle forces arising from adsorbed polyelectrolytes in colloidal suspensions. *Colloids and Surfaces A: Physicochemical Engineering Aspects, 95*, 43–52.

Leong, Y. K., Du, M., Au, P. I., Clode, P. L., & Liu, J. (2018). Microstructure of sodium montmorillonite gels with long aging time scale. *Langmuir, 34*, 9673–9682.

Mizuno, H., Luengo, G. S., & Rutland, M. W. (2010). Interactions between crossed hair fibers at the nanoscale. *Langmuir, 26*, 18909–18915.

Murray, H. H. (2000). Traditional and new applications for kaolin, smectite, and palygorskite: A general overview. *Applied Clay Science, 17*, 207–221.

Neaman, A., & Singer, A. (2000). Rheology of aqueous suspensions of palygorskite. *Soil Science Society of America Journal, 64*, 427–436.

Nègre, M., Leone, P., Trichet, J., Défarge, C., Boero, V., & Gennari, M. (2004). Characterization of model soil colloids by cryo-scanning electron microscopy. *Geoderma, 121*, 1–16.

Nguyen, Q. D., & Boger, D. V. (1985). Direct yield stress measurement with the vane method. *Journal of Rheology, 29*, 335–347.

Norrish, K., & Rausell-Colom, J. A. (1962). Effect of freezing on the swelling of clay minerals. *Clay Minerals Bulletin, 5*, 9–16.

Odriozola, G., Romero-Bastida, M., & Guevara-Rodríguez, F.d. J. (2004). Brownian dynamics simulations of Laponite colloid suspensions. *Physical Review E, 70*, 021405.

Ruiz-Hitzky, E. (2011). Molecular access to intracrystalline tunnels of sepiolite. *Journal of Materials Chemistry, 11*, 86–91.

Ruzicka, B., Zaccarelli, E., Zulian, L., Angelini, R., Sztucki, M., Moussaïd, A., Narayanan, T., & Sciortino, F. (2011). Observation of empty liquids and equilibrium gels in a colloidal clay. *Nature Materials, 10*, 56–60.

Sabah, E., Mart, U., Çınar, M., & Çelik, M. S. (2007). Zeta potentials of sepiolite suspensions in concentrated monovalent electrolytes. *Separation Science and Technology, 42*, 2275–2288.

Sehly, K., Chiew, H. L., Li, H., Song, A., Leong, Y. K., & Huang, W. (2015). Stability and ageing behavior and the formulation of potassium-based drilling muds. *Applied Clay Science, 104*, 309–317.

Shu, R., Sun, W., Liu, X., & Tong, Z. (2015). Temperature dependence of aging kinetics of hectorite clay suspensions. *Journal of Colloid and Interface Science, 444*, 132–140.

Simonton, T. C., Komarneni, S., & Roy, R. (1988). Gelling properties of sepiolite versus montmorillonite. *Appied Clay Science, 3*, 165–176.

Solomon, M. J., & Boger, D. V. (1998). The rheology of aqueous dispersion of spindle-like colloidal hematite rod. *Journal of Rheology, 42*, 929–949.

Suman, K., & Joshi, Y. M. (2018). Microstructure and soft glassy dynamics of an aqueous Laponite dispersion. *Langmuir, 34*, 13079–13103.

Tunc, S., Duman, O., & Cetinkaya, A. (2011). Electrokinetic and rheological properties of sepiolite suspensions in the presence of

hexadecyltrimethylammonium bromide. *Colloids and Surfaces A: Physicochemical Engineering Aspects, 377*, 123–129.

Wolf, B., White, D., Melrose, J. R., & Frith, W. J. (2007). On the behavior of gelled fiber suspensions in steady shear. *Rheologica Acta, 46*, 531–537.

Yoon, J., & El Mohtar, C. (2013). Dynamic rheological properties of sodium pyrophosphate modified bentonite dispersions for liquefaction mitigation. *Clays and Clay Minerals, 61*, 319–327.

Zhang, J., Yan, Z., Ouyang, J., Yang, H., & Chen, D. (2018). Highly dispersed Sepiolite-based organic modified nanofibers for enhanced adsorption of Congo red. *Applied. Clay Science, 157*, 76–85.

(Received 19 July 2019; accepted 3 December 2019; AE: George D. Chryssikos)